Space Microgrids: New Concepts on Electric Power Systems for Satellites

Lashab, Abderezak; Yaqoob, Mohammad; Terriche, Yacine; Vasquez, Juan C.; Guerrero, Josep M.

Published in:
I E E E Electrification Magazine

DOI (link to publication from Publisher):
10.1109/MELE.2020.3026436

Publication date:
2020

Document Version
Accepted author manuscript, peer reviewed version

IEEE Electrification Magazine

Space Microgrids: New Concepts on Electric Power Systems for Satellites

Abderezak Lashab, *Member, IEEE*, Mohammad Yaqoob, *Student Member, IEEE*, Yacine Terriche, *Student Member, IEEE*, Juan C. Vasquez, *Senior Member, IEEE*, and Josep M. Guerrero, *Fellow, IEEE*

Abstract: The electric power systems (EPSs) are of a paramount importance in satellites. These systems are responsible for power generation, storage, delivery, and conditioning. A failure in an EPS may hinder all the aforementioned functionalities, which consequently, leads to a failure of the whole space mission. There are many technologies available in both industry and literature of EPSs, where each has its own fault tolerance capabilities. On the other hand, the efficiency of the EPS is an important factor, which promotes having higher power reserve; thus, feeding the payloads at all needed times. In this paper, the EPS for Satellites-based microgrids are reviewed with more focus on their energy generation and storage, including their protection schemes. Moreover, sizing guidelines for the energy generation and storage systems are also provided.

I. Introduction

Satellites are an emerging technology, which is being employed in many unique applications, such as space science and exploration, high speed internet, ships and airplanes tracking, etc 0as mentioned in the articles of J. Bouwmeester et al. and A. Aoudeche et al. published in 2010 and 2018, respectively. Nevertheless, satellites require a knotty design, burdened by tradeoffs, which are very disingenuous to balance in this specific application. Among those are the space craft development time and price, including the lunch ones. In order to over the deficiencies of the above mentioned satellites, small satellites such as nanosatellites and picosatellites, or else known as CubeSats, have been proposed and developed to mitigate from the aforementioned burdens, resulting in different space craft classes, as shown in TABLE 1. This class of satellites orbit in the low earth orbit (LEO), and are therefore able to perform most of the tasks corresponding to larger satellites. Moreover, they orbit in low orbits of other

TABLE 1. Classification of spacecraft with mass and manufacturing time by P. Bugryniec, 2016.

Type	Mass (kg)	manufacturing time (years)
Large-satellite	>1000	>5
Medium-satellite	500 - 1000	4
Mini-satellite	100 - 500	3
Micro-satellite	10 - 100	1
Nano-satellite	1 - 10	<1
Pico-satellite	0.1 - 1	<1
Femto-satellite	<0.1	<1

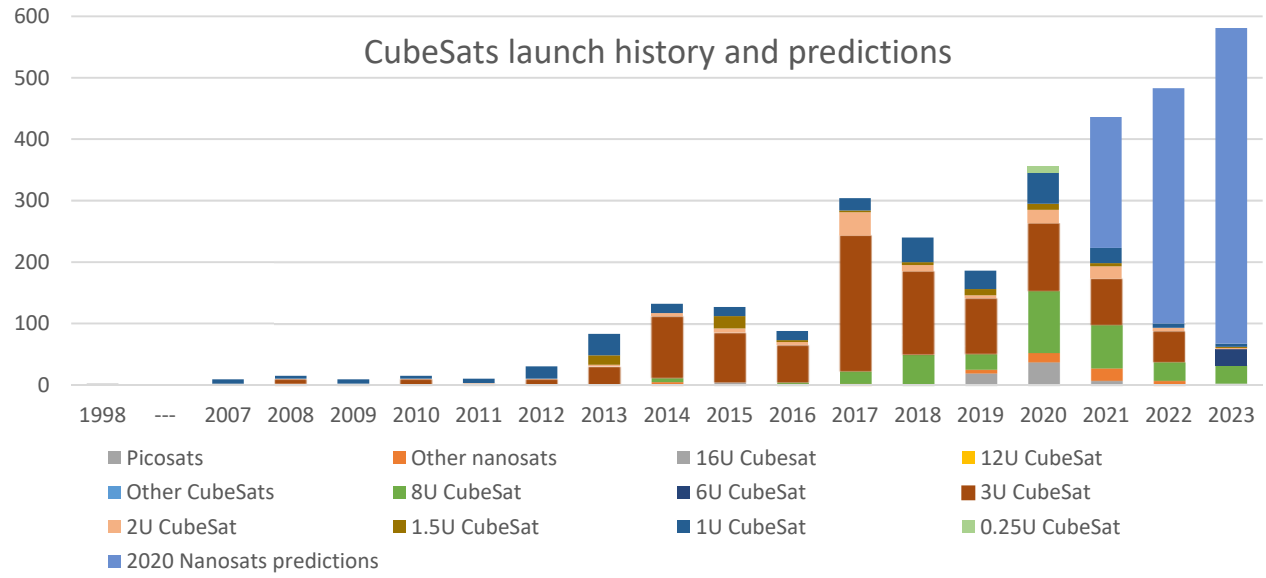

Fig. 1. CubeSats launch history and predictions with respect to different sizes, E. Kulu, 2020.

planets like Mars as stated in the publication by T. Komarek et al. in their 2013 article. CubeSats are modular and scalable, where the basic unit weights 1.33kg or less and occupies an area of 10cm×10cm×10cm. This modular structure allows having a larger satellite with higher-level capabilities, while a simple structure and design are still advantages. The need for such a small-scale satellite began to be evident as a result of research and investigations done at Stanford University's Space System Development Laboratory in 1998. The first CubeSats were a pair of Picosats tied together by a short wire, launched from an OPAL Launch System on February 8, 2000. With the developments of more miniaturized components, CubeSats continued to evolve even more than before, as shown in Fig. 1, which is given in the data base by E. Kulu in 2020.

The EPS is one of the main composites of the satellites, which works on the power generation, storage, delivery and conditioning. Without any of those, the satellites would be out of service and may cause the failure of the whole space mission. The EPS of the satellite has attracted great attention of researchers due to the number of stringent requirements, such as limited weight and space, impossible repair, a wide range of temperatures and severe radiation environment. These requirements can be fulfilled by sophisticated control methods, and robust and resilient design of the EPS. Lee et al. have presented the design and management of satellite power systems, where they have investigated the demand, characteristics, management, and design to meet the required goals of the satellite power supply. This study has followed an actual nano-satellite by demonstrating some effective solutions as a case study. Timothy et al. 0have presented a modular EPS architecture for LEO satellites. The main idea is modularization to make the EPS reusable for a variety of missions with a minimal redesign. In this context, the energy generation and storage subsystems are modularized and the objectives of the

modularization are accomplished with no compromise on the power stability and efficiency. Furthermore, for a case study of the CubeSat KySat-2, calculations were performed for determining the overall efficiency of the system, where the efficiency is 71.07% when all the payloads were connected to the modular EPS. In 2019, Djebko et al. 0have presented a model-based fault detection and diagnosis for the power supply of the SONAT triple cube nano-satellite. In this study, for the abnormal behavior of the components, a generic model-based diagnosis system is presented, which detects the abnormality to take countermeasures earlier. The observed data of the components and the housekeeping data are analyzed through simulation and the expected behavior of the component is then attained. The experimental results show that this fault detection system detects the abnormality, which is not predictable by telemetry data only. Pang et al. 0identified a robust scheduling and design of nanosat swarm based on bandwidth limit and power budget for synthetic aperture radar (SAR) applications in their 2015 article. Here, considering stochastic failure a robust and energy efficient scheduling is proposed and effectiveness of the scheduling is confirmed with mathematical rigor and simulations. The simulation results show acceptable mean total energy consumption, improvement in the meantime to mission failure, and meantime between failures. Moreover, Bester et al. have designed a photovoltaic (PV)-battery based EPS for a 3U CubeSat, applying peak power trackers for the regulation of the solar array and battery charging. By applying a unique search algorithm, Perturbed and Observe (P&O) power tracking is executed in both digital and analogue arrangement constructing an efficient EPS with built-in redundancy. Anwar et al. have proposed a design of EPS and attitude determination and control system (ADCS) for a standard CubeSat on a single tile. This design offers an inventive solution for many constraints like power consumption, physical measurements and cost. Additionally, beside the cost and weight reduction of the EPS, this design provides more space to accommodate additional subsystems.

II. Overall CubeSat Structure

Fig. 2 shows the overall schematic of the EPS for satellites. For the energy generation, PV cells are employed, where the electrical parameters “voltage and current” of these cells are sensed and then sent to the control circuit or microprocessor. Based on these measurements, the controller estimates the voltage corresponding to the maximum power point (MPP) of the cells, and drives the input voltage of the boost to this operating point as detailed in several publications like, A. Lashab et al. in their 2019, and 2020 publications, respectively. The power harvested by the PV cells is delivered both to the payloads and battery. The energy stored in this latter is a backup for the CubeSat during the eclipse when the satellite goes to the dark side of the planet “or orbit” where the PV cells get shaded. The energy stored in the battery might be used during peak loads, even when the CubeSat is subjected to the sun. In CubeSat class, the battery could be paralleled directly to the main bus, or interfaced to that latter through a bidirectional converter, as shown in Fig. 2. The former configuration features higher efficiency; but has less flexibility in term of battery voltage with respect to the second one.

Moreover, for the attitude control of the satellite, it is equipped with a gyroscope, magnetometer, and a magnetorquer, as mentioned in the publication of M. Schmidt et al., 2008. The gyroscope is responsible for measuring and controlling the CubeSat in term of angular velocity. Since the COTS gyroscope

intended for CubeSat application operate with 5V and 3.3V, respectively, the main bus is regulated to this voltage levels through switching regulators, as shown in Fig. 2. The magnetometer is employed in CubeSats since they orbit in LEO, where the interactions with the Earth magnetic file are possible for controlling the satellite orientation. In addition to the voltage needed for the gyroscope, the magnetometer requires an extra regulated 3V, as detailed in S. P. Viswanathan et al. in their 2016 article. Regarding the magnetorquer, it generates a magnetic dipole that interacts with the Earth's magnetic field "or other

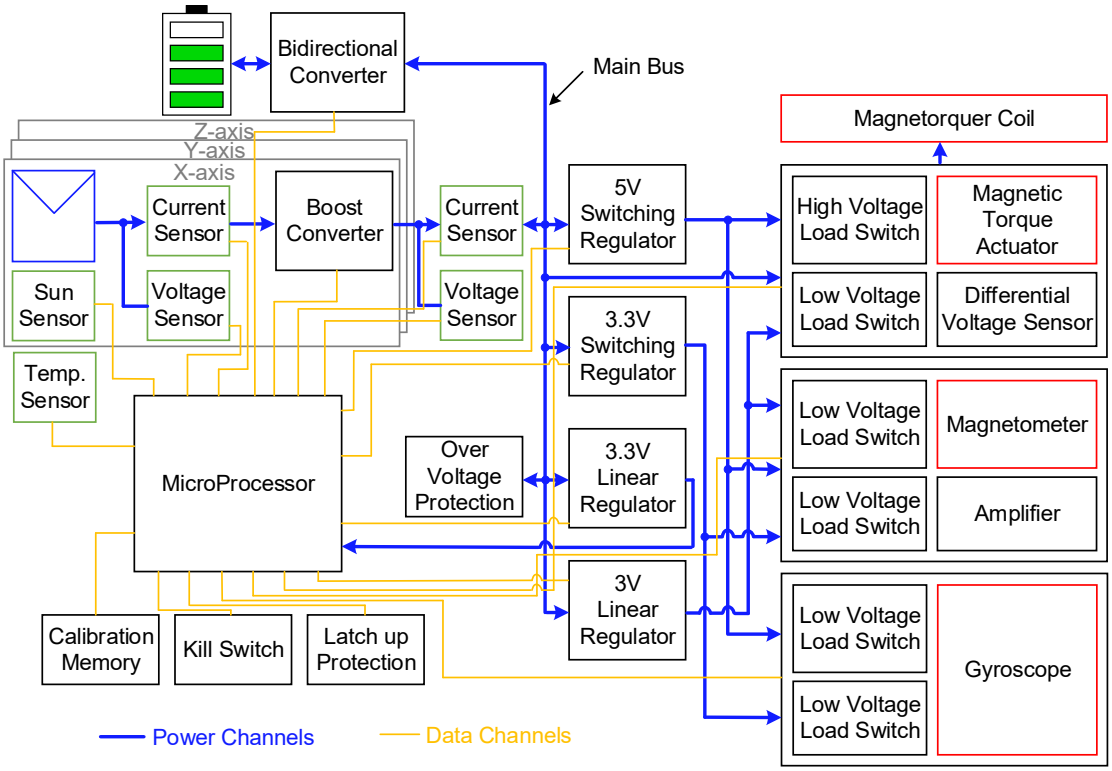

Fig. 2. The overall structure of the CubeSat.

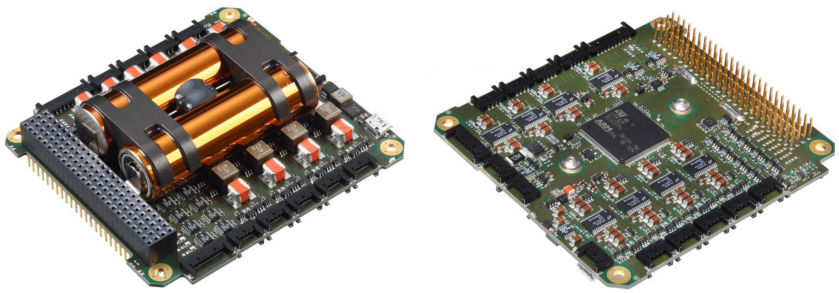

(a) (b)

Fig. 3. Nano Avionics EPS: (a) the top view; (b) the bottom view.

planet being orbit around to", in a way that the magnetic force generated creates the intended torque for the satellite stabilization, as stated in the thesis of C. Kaplan. This magnetorquer operates under a regulated 5V and 3V, besides the unregulated main bus voltage.

The main bus is connected to an overvoltage protection device. Moreover, each load is linked to a protection circuit which shuts down the corresponding load if it draws a current that is at a higher level than the maximum specified one for that load. This may occur if the load suffers from an internal latch-up caused by radiation effects. The CubeSat employs also a kill switch, or else known as the emergency-stop. This latter works on turning off the satellite in case of an emergency situation. The difference between the kill switch and the normal shutdown is that the former is quicker, simpler, and works in a non-orderly fashion even if this damages some equipments.

III. Energy Generation in the CubeSat

As mentioned earlier, for the energy generation, CubeSats are, in most of the cases, equipped with PV solar cells, although there are other developments, such as radioisotope technology in interplanetary missions, as presented in the iCubeSat workshop by E. Wertheimer et al.. Among the available PV solar cells technologies, the triple junction one (GaInP/GaAs/Ge) is the most adopted in CubeSats due to its higher efficiency with respect to the silicone (Si)-based considering the surface that it occupies on the satellite. This can be seen in Fig. 4, which shows a comparison between commercial Si- and GaInP/GaAs/Ge-based solar cells. This is due to the fact that this junction combination captures longer wavelength, as depicted in Fig. 5. As can be seen from the chart in Fig. 4, this technology operates under higher voltage compared to the Si-based one, which is more convenient from the interfacing power converter design standpoint.

The efficiency of the solar cells can be improved further by using the concentrator. The concentrator uses lenses and curved mirrors to focus and direct the solar irradiance onto the multijunction solar cell. In this way, the efficiency of the solar cell can be improved at minimal additional cost as compared to using a different solar cell chemistry. Some examples of solar cells with concentrators are shown in Fig. 6(b) and (c).

Regarding the solar PV cells modelling, the one diode model is known, and combines simplicity with fairly accurate PV solar cell behavior estimation, as detailed in the publications of M. G. Villalva et al. and A. Lashab et al., 2009 and 2015, respectively. The power generated by the solar cell is mainly influenced by the solar irradiance (G), the temperature (T), and the solar radiation incident angle (θ), as:

$$P_{PV}=P_s\,\eta_{Sun/PV}\,K_G\,K_T\,K_R \tag{1}$$

where P_s is the sun received power on the cell surface, $\eta_{Sun/PV}$ is the PV cell efficiency, K_G is solar irradiance factor, K_T is the temperature factor, and K_R is the reflection loss factor. The temperature factor can be estimated as

$$K_T = 1 + \alpha(T_i - T_{STC}) \tag{2}$$

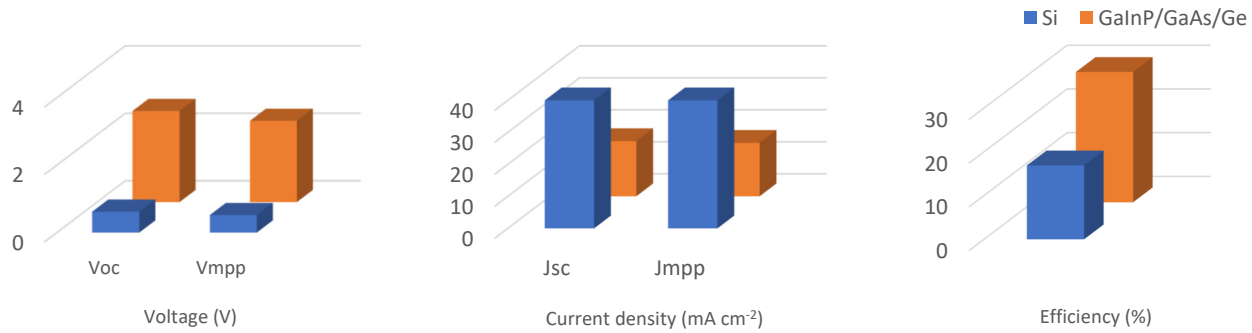

Fig. 4. Comparison between the Si (S32) and GaInP/GaAs/Ge (TJ Solar Cell 3G30C) solar cells in terms of voltage, current over surface, and efficiency.

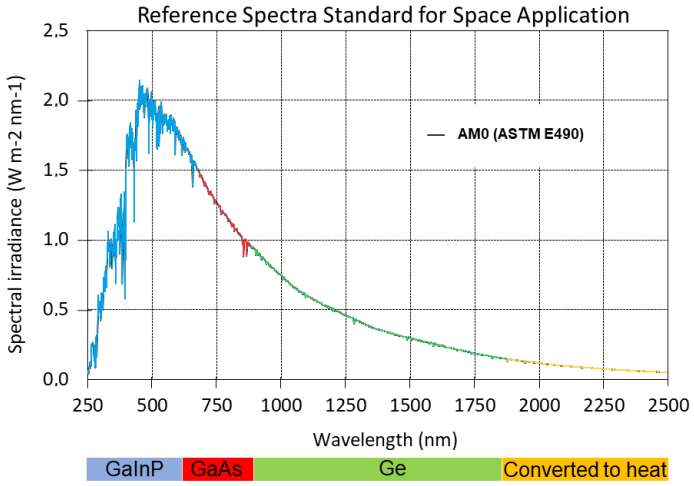

Fig. 5. AM 0 solar spectrum captured by the different PV solar cell junctions.

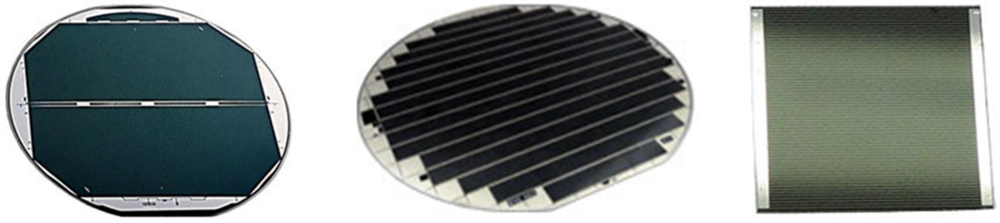

(a) (b) (c)

Fig. 6. (a); Triple Junction Solar Cell ($\eta_{Sun/PV}$ =32%) (b); C3MJ–Lattice matched 3J metamorphic PV cell ($\eta_{Sun/PV}$ =39.5%) (c) C4MJ–Upright 3J metamorphic PV cell ($\eta_{Sun/PV}$ =40%). All from Spectrolab.

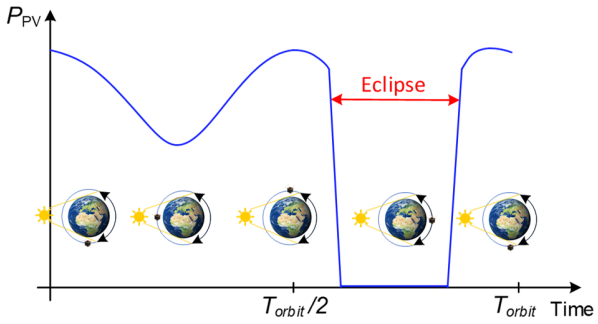

Fig. 7. The PV power profile during one orbit.

such as, α is the temperature coefficient, T_i is the instantaneous temperature and T_{AM0} is the temperature at the AM0 conditions (28°C). Regarding the reflection loss, it can be estimated as

$$K_R = \cos(\theta) \tag{3}$$

The solar radiation incident angle θ is the one between the perpendicular line to the cell surface and the solar radiation line. If this angle reaches 50° or beyond, the actual response can be represented accurately using Kelly's cosine law.

The nominal performance data, such as open circuit voltage (v_{OC}), maximum power voltage (v_{MPP}), short circuit current (i_{SC}), and maximum power current (i_{MPP}), of PV solar cells for space applications are provided according to AM0 (28°C). These solar cells are usually serially connected to increase their voltage level to become $v = n_s \times v_{PV}$ (n_s is the number of serially connected solar cells). This scaling is usually referred to as a PV solar string. To increase the current level, multiple strings are paralleled so that the delivered current becomes $i = n_p \times i_{PV}$ (n_p is the number of paralleled PV solar cells or strings).

The solar generated power is largely affected by the solar irradiance and temperature, as expressed by (1), where this power is proportional to the solar irradiance and inversely proportional to the temperature. Accordingly, the generated power is null during the eclipse, while it is variable during the sunlight, as shown in Fig. 7. As it can be seen from this figure, the generated power decreases when the satellite approaches the sun since the temperature is higher there.

IV. Energy Storage in the CubeSat

For a continuous operation of the CubeSat, batteries are employed as a backup, which are charged during high solar irradiance levels when the power generated by the solar arrays is higher than the loads one. The batteries are used for the eclipse duration, as well as under the high solar irradiance levels during the peak loads. The size and technology of batteries for satellites are selected based on the capacity and

power delivery requirements, temperature ranges, number of expected service cycles, and physical size and weight. Due to these factors, nickel cadmium (NiCd) has been widely used in CubeSat missions, as presented in the iCubeSat workshop by E. Wertheimer et al.. Nevertheless, this battery technology has been replaced by the lithium-ion (Li-ion) one since it offers higher energy density, higher operating voltage, and higher service cycles and reliability in general, as detailed in M. Robyn et al.'s publication in 1995.

The integral of the current over time is defined as the *nominal capacity* (*C*) of the battery in the battery's terminology, and its symbolized unit is referred to as Ampere-hour or Ah. This current integral is from the fully charged battery state to the fully discharged one, at room temperature. In other words, the battery capacity is the indication of the *C* ampere that the battery is able to deliver in one hour, and in some cases, it is expressed in *C/n*, which means the *C* ampere in *n* hours. Regardless of the battery chemistry, their capacity degrades with the count of charge/discharge cycles, the quantity of charge change in each cycle, discharge current, and temperature. With regards to the discharge and charge current, it is usually indicated to as the *C*-rate, where 1*C* is the current under which the battery would charge or discharge in one hour. In most of the cases, the Li-ion batteries charge and discharge under a maximum current level of 1*C*; nevertheless, there have been some developments on this type of batteries where they are able to discharge under 2*C* or higher. To obtain the nominal battery energy, its nominal voltage is multiplied by its capacity, and its unit symbol is Watt-hour or Wh.

Similar to the case of the PV cells, batteries operate under low voltage, and they are, therefore, serially connected to increase the operating voltage, forming a battery string, while to further increase the capacity, i.e. current, these strings are paralleled.

During the selection process of the battery for a space mission, several factors need to be taken into account in order to have an estimate of the battery's end-of-life (EOL). Among these factors, the number of charge and discharge cycles of the battery, especially in satellites orbiting in LEO, as their number of cycles could reach up to 16 cycle per day. The depth of discharge (DOD), which indicates the percentage of how much energy can be used from the battery is another factor. To estimate the battery's DOD, the deliverable capacity is usually divided over the total one, as $\mathrm{DOD}=C_{\mathrm{deliverable}}/C$. Another way is to estimate the battery's state-of-charge (SOC), which defines what is the minimum SOC that the battery could bear without any risk of getting damaged, as $\mathrm{SOC}=C_{\mathrm{minimum}}/C$. A large SOC, or short DOC helps in improving the battery's life-time; but, that would be at the expense of a larger size occupying battery. DODs ranging between 30% to 50% are usually selected, which are in accordance with the manufacturer recommendations. Other factors of paramount importance are the battery maximum charge voltage, or else known as the end-of-charge (EOC) voltage, and the minimum discharge voltage, or else known as the end-of-discharge (EOD) voltage. Any violation of these voltage levels would cause deformations in the electrochemistry of the battery, which significantly affects its life-time, negatively. These voltage limits are displayed in Fig. 8 together with the battery nominal voltage. The energy injected into the battery is not all recovered due to the electrochemical process involved, as well as due to its internal impedance. Accordingly, the battery is characterized also by its energy efficiency ($\eta_{\mathrm{BT\text{-}CH/DCH}}$), which varies from one technology to another. Finally, the energy that the battery stores with respect to its weight, known as the gravimetric energy density (Wh kg^{-1}), as well as its storable energy with respect to

its size, known as the volumetric energy density (Wh l^{-1}), are other key factors that are, usually, taken into account when selecting the right battery for the mission.

It is important to note that, the DOD of the battery varies in the whole range, i.e. from 0 to 100%, when the battery voltage is in the regions with lower steepness, which are corresponding to the nominal voltage (see Fig. 8). As it can be seen also from this figure, the battery charges under a randomly changing positive current, where the level of this latter is dependent of the harvested PV power and consumed one. Once the battery voltage reaches v_{EOC}, the battery charge control shifts to voltage mode in order to not overpass this limit, while keeping the battery charge at the maximum. In practice, the battery would still consume some current, as shown in Fig. 8, even when it is fully charged due to the fact that it loses some of the stored energy. During the discharging phase of the battery, it shifts again to current mode, where the current value is determined based on the difference between the harvested PV power and the load demand.

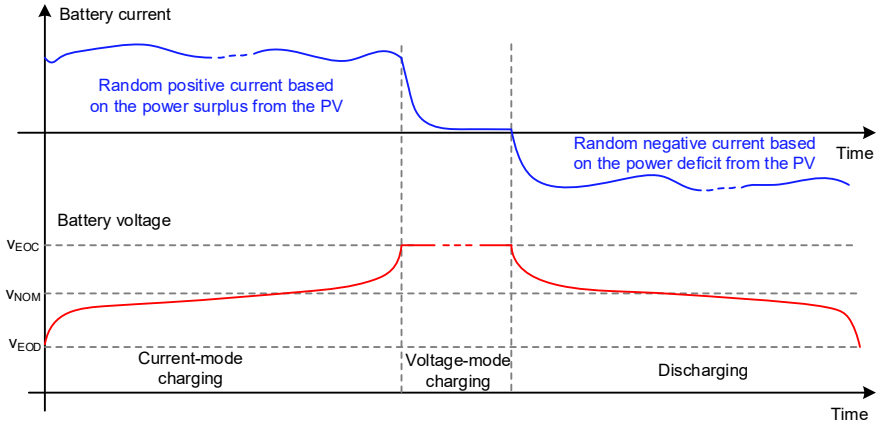

Fig. 8. A typical Li-ion battery charging and discharging characteristic.

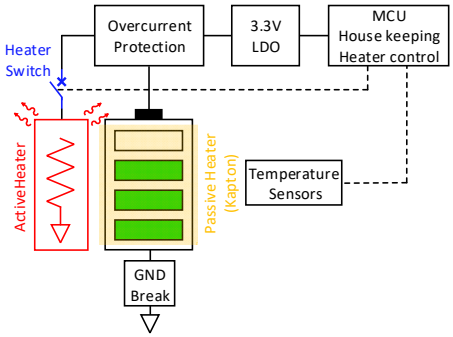

Fig. 9. A simplified thermal management schematic of battery for satellites.

Onboard the satellite, the most constrained element by the temperature range is the battery, even if it is not being used (neither charging nor discharging), as it is elaborated by S.-J. Kang et al. in their 2016

article. Moreover, despite using the battery in the allowed range, its performance degrade as the temperature goes toward one of the extreme limits (very hot or very cold). Under low temperatures the battery internal resistance increases, which worsens the power losses. If the temperate goes even lower, the battery internal resistance may increase to a point where its discharging becomes challenging. Accordingly, batteries for satellites are equipped with both passive and active heaters. For the former, Kapton film is wrapped around the battery in order to maintain its temperature at average levels and as steady as possible. For the active heater, resistor-based ones are usually used, as depicted by Fig. 9. As it can be seen from this figure, this heater is fed from the battery its self, where these two are interfaced through the overcurrent protection circuit and a heater switch. The overcurrent protection circuit is the same interfacing either the battery converter or the main bus depending on the adopted configuration. Regarding the heater switch, it is controlled through a microcontroller unit (MCU), which is programmed for the battery housekeeping and heater control. This MCU is also fed by the battery its self through a 3.3V low dropout (LDO) voltage regulator, as shown in the same figure.

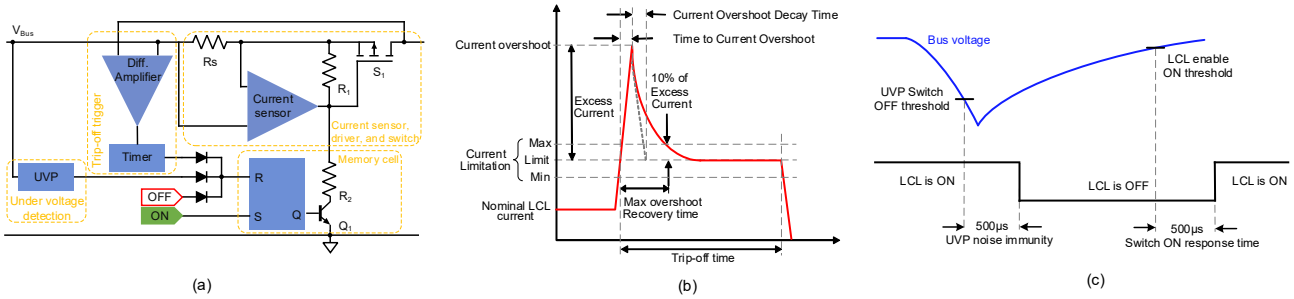

Fig. 10. An LCL diagram including UVP: (a) Typical diagram; (b) overcurrent event; (c) undervoltage event.

V. EPS Protection on the CubeSat

A typical diagram of a latch-up current limiter (LCL), together with an undervoltage protection (UVP) is shown in Fig. 10(a). The combination of the LCL with the UVP is referred to as the *protection unit* thereafter. As detailed in G. F. Volpi' publication of 2007, the protection unit is usually placed between the load and voltage regulator0. It consists of a switch with its driver, current sensor, trip-off trigger, under voltage detector, and a memory cell. The protection unit can be ON or OFF, and this is usually determined by the memory cell.

The protection unit switch might be triggered by either a signal coming from the current sensor, which identifies if the current level has exceeded the predefined limit as a consequence of an overload or fault, or by the reading of the differential voltage across the switch (as shown in Fig. 10(a)).

A. Latch-up current limiter (LCL)

In the case of an overload or a fault in the load, when the current of the latter goes higher than a predetermined threshold, the LCL changes its mode of operation into current limitation. At the beginning of this event, the timer shown in Fig. 10(a) is activated. This timer counts for a duration called as the

trip-off time, as long as the current absorbed by the load is still higher than its predefined threshold. During this mode of operation, the switch S_1 is forced to operate in the linear mode instead of operating in the ohmic "ON" mode. This mode change at the level of the switch S_1 should be quick in order to decrease from the surge current. The current sensor is responsible for controlling the load current in this mode to a lower and fixed level, as shown in Fig. 10(b), which is achieved by modulating the switch S_1 gate voltage. The accuracy of this latter is dependent upon the voltage reference used in the design and current sensing circuit. Note that, the current sensor, in some cases, is also employed to acquire the current telemetry signal. If this mode of operation continues until the trip-off time elapses, then the timer would command the protection unit to shut off the load, as depicted in Fig. 10(b).

It is noteworthy that, depending on the load current and equivalent inductance, the LCL may be coordinated with a provision circuitry in order to allow the freewheeling of the current. This scheme can be achieved by adding an anti-parallel diode at the output of the protection unit.

B. Under voltage protection

In case the bus voltage goes lower than the predefined value, e.g. due to unbalance between the power flown into the bus and the one required by the loads, the UVP triggers the memory cell. Consequently, the bus voltage recovers its voltage level, as illustrated in Fig. 10(c). As it can be also noted from this figure, the UVP shuts down and turns on the protection unit with a hysteresis, where the aim of this process is to avoid any possible noise effects. This could be the case especially in unregulated bus schemes.

The UVP could be implemented in a centralized manner, where the shut down signal is sent to different LCL switches, or in a distributed one where each LCL switch has its own UVP. Nevertheless, the centralized UVP is more challenging compared to the distributed one, since in the former, the single point failure free (SPFF) feature needs to be incorporated in it so that not all LCL switches are turned off, especially those of critical loads, which may lead the spacecraft to deviate from its orbit, or other high level risks.

VI. Sizing of the Electric Power System in the CubeSat

As mentioned earlier, the CubeSat can generate the power during a limited time, which is before going into eclipse again during its periodic cycle. Moreover, the load demand in the satellite may overpass the power generated by the PV cells, even if the satellite is not in eclipse. Accordingly, the energy balance in the battery, with some positive margin, is one of the vital design criteria for the battery in the EPS.

Regarding the overall power, the CubeSat's EPS should meet the energy balance given by the following

$$E_{PV}=E_{load}^{sun}+E_{CHG}+E_{loss}^{sun}+E_{loss}^{eclipse} \tag{4}$$

where E_{PV} is the PV cells harvested energy, E_{CHG} is the energy needed to recharge the battery, E_{loss}^{sun} is the energy lost in the power system under the sunlight, and $E_{loss}^{ecliplse}$ is the energy lost in the power system

under the sunlight. Note that, E_{CH} is the same as the load demand during the eclipse $E_{load}^{eclipse}$ including the energy lost for recovering it.

$$E_{\mathrm{CH}} = \frac{E_{\mathrm{DCH}}}{\eta_{\mathrm{BT}}} \tag{5}$$

such as E_{DCH} is the energy that should be recovered from the battery. This energy balance is deemed for a single orbit period. Accordingly, the energy balance as function of the power can be written as follows

$$E_{\mathrm{PV}} = \int_{t_{\mathrm{ini}}}^{t_{\mathrm{ini}}+t_{\mathrm{eclipse}}} P_{\mathrm{PV}}(\mathrm{t})\, dt \tag{6}$$

$$E_{load}^{sun} = \int_{t_{\mathrm{ini}}}^{t_{\mathrm{ini}}+t_{\mathrm{eclipse}}} P_{load}^{sun}(\mathrm{t})\, dt \tag{7}$$

$$E_{loss}^{sun} = \int_{t_{\mathrm{ini}}}^{t_{\mathrm{ini}}+t_{\mathrm{eclipse}}} P_{loss}^{sun}(\mathrm{t})\, dt \tag{8}$$

$$E_{loss}^{eclipse} = \int_{t_{\mathrm{ini}}+t_{\mathrm{eclipse}}}^{t_{\mathrm{sun}}} P_{loss}^{eclipse}(\mathrm{t})\, dt \tag{9}$$

where t_{sun} is the time at which the CubeSat starts to be subjected to solar irradiance, and t_{eclipse} is the time at which the CubeSat starts to be in eclipse.

C. Load Demand

Among the primary tasks in EPS sizing is determining a detailed load demand profile for the whole satellite, as well as for each subsystem to be fed (see Fig. 11). Separate load demand profiles for both sunlight and eclipse and sunlight periods are key factors for the estimation of the energy generation and storage sizing. Furthermore, the energy losses corresponding to the EPS's different power flows are other factors with an important impact in this matter. Peak and average load demands for each subsystem need also to defined. Alternatively, the ratio (R_{p}) between the average power and the peak one over a period of time is usually referred to characterize the load demand

$$R_P = \frac{\int_{t_{\mathrm{ini}}}^{t_{\mathrm{ini}}+T_{orbit}} P_{load}(\mathrm{t})\, dt}{P_{load}^{peak}\, T_{orbit}} \tag{10}$$

where T_{orbit} is the orbit duration.

D. Orbit and eclipse durations

Both the orbit and eclipse durations are of very paramount importance when sizing the solar array and battery. To calculate the duration of the eclipse in the LEO circular orbit, the third law of Kepler for planetary motion can be applied, which provides the period of the eclipse as function of the orbit duration,

$$T_{eclipse} = \frac{T_{orbit}}{2} - \frac{T_{orbit}\cos^{-1}\left(\frac{R_o - h}{R_o}\right)}{\pi}; \text{ where } T_{orbit} = \sqrt{\frac{4\pi^2 R_o^{\,3}}{G_{Earth} M_{Earth}}} \tag{11}$$

where R_o is the radius of the orbit, h is the altitude of the orbit, G_{Earth} is a gravitational parameter (G_{Earth}=6.67×10^{-11} Nm^2/kg^2), and M_{Earth} is the Earth's mass (M_{Earth}=5.94 ×10^{24} kg).

In the case of CubeSats orbiting in LEO, the duration of the eclipse varies according to the sunlight incident angle with respect to the orbit plane—which takes different values upon the present season, as well as the orbit altitude and inclination. Accordingly, in LEO, the eclipse duration may get doubled compared to its minimum duration. Moreover, the ratio between the duration of the eclipse and the total orbit play an important role as it influences the PV array, battery, and other EPS elements requirements.

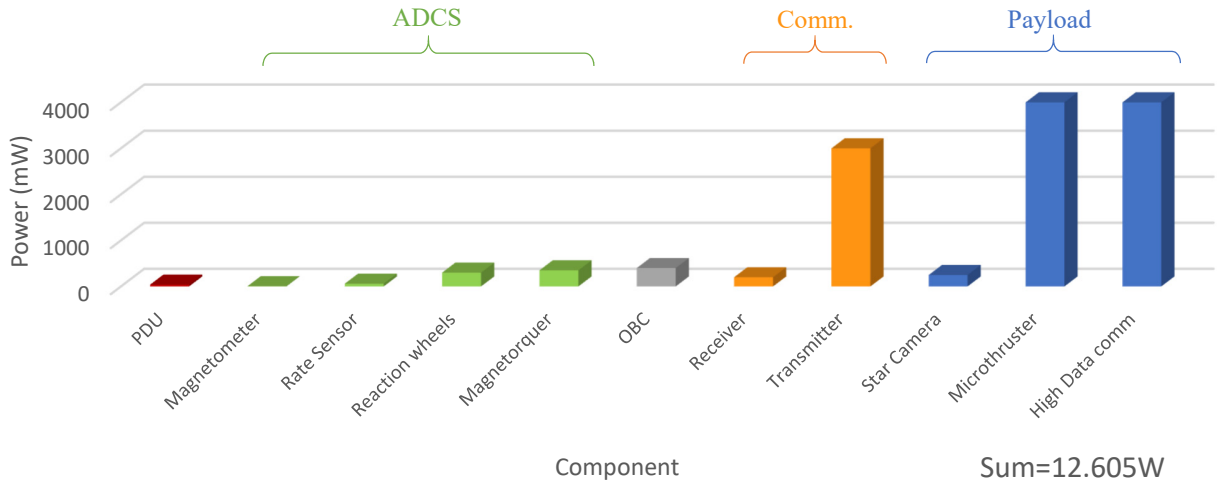

Fig. 11. Sample power demand for YUsend-1, N. Navarathinam et al., 2011.

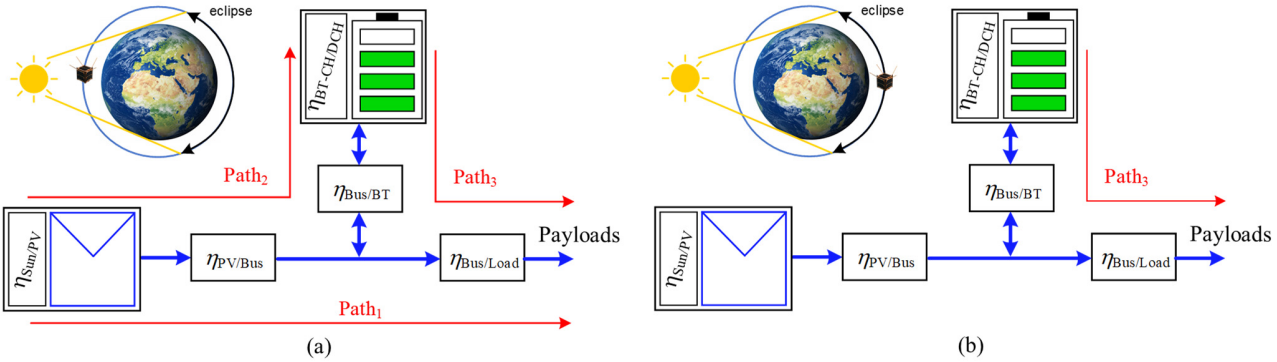

Fig. 12. The power paths and energy efficiency of the power generation, storage, distribution, and conditioning subsystems, during (a) the sunlight and (b) eclipse durations.

E. Power Losses Estimation

The generation, storage, distribution, and conditioning of the electrical energy are performed at some expenses, among which are the power losses. In order to estimate the power losses dissipated in the EPS during the mission, the power flow throughout the EPS needs to be identified during both the sunlight and eclipse durations. Moreover, the efficiency of each individual generation, storage, distribution, and conditioning subsystem need to be accurately defined.

For performing the above-mentioned study, the system in Fig. 2 can be redrawn in terms of power paths and efficiency as shown in Fig. 12. As it can be seen from this figure, there are three power paths, $Path_1$, $Path_2$, and $Path_3$, which are namely from the PV array to the payload, from the PV array to the battery, and from the battery to the payloads, respectively. These paths are representing the case of injecting power directly from the PV array to the payloads during sunlight, the case of injecting the excess of power from the PV arrays to the battery during sunlight, and the power backup from the battery to the payloads during eclipse. Regarding the efficiencies, $\eta_{\text{Sun/PV}}$ represents the efficiency of the PV array when transferring the sun light into electrical energy, while $\eta_{\text{PV/Bus}}$ represents the efficiency from the solar cell to the main bus, which includes the solar cell series and shunt resistor losses, antiparallel diode loss, and boost converter losses. $\eta_{\text{Bus/BT}}$ represents the efficiency of the path from the bus to the battery, which includes the bidirectional converter power losses (in the case of regulated bus), battery diodes, and battery protection switches, while $\eta_{\text{BT-CH/DCH}}$ represents the efficiency of the battery its self, due to the electrochemical reactions and lost stored energy. $\eta_{\text{Bus/Load}}$ summarizes the power lost in the power conditioning modules (PCMs), payload switches, and latch-up protection devices. Other power losses due to the supply of the voltage, current, and temperature sensors, as well as of the integrated circuits might be included in the efficiency evaluation for a higher accuracy.

By coordinating between the aforementioned paths and efficiencies, the following can be concluded. During eclipse, the direct path, $Path_1$ for feeding directly the payloads from the PV array and $Path_2$ for charging the battery, and both $Path_2$ and $Path_3$ for storing and recovering power for high-power pulsed loads, are where the power flows. Accordingly, the power loss during this time interval can be expressed as

$$E_{loss}^{Sun} = E_{load}^{Sun}\left(E_{lossPath1} + \frac{E_{lossPath2}\,E_{lossPath3}}{\eta_{\text{BT-CH/DCH}}}\right) + E_{load}^{ecliplse}E_{lossPath2} \tag{12}$$

where $E_{lossPath1}$, $E_{lossPath2}$, and $E_{lossPath3}$ summarize the energy lost in the paths, which can be expressed as function of the efficiencies as

$$E_{lossPath1} = \frac{1-\eta_{\text{PV/Bus}}\eta_{\text{Bus/Load}}}{\eta_{\text{PV/Bus}}\eta_{\text{Bus/Load}}};\; E_{lossPath2} = \frac{1-\eta_{\text{PV/Bus}}\eta_{\text{Bus/BT}}}{\eta_{\text{PV/Bus}}\eta_{\text{Bus/BT}}};\; E_{lossPath3} = \frac{1-\eta_{\text{Bus/BT}}\eta_{\text{Bus/Load}}}{\eta_{\text{Bus/BT}}\eta_{\text{Bus/Load}}} \tag{13}$$

While during the eclipse the power losses can be estimated as

$$E_{loss}^{eclipse} = E_{load}^{eclipse} \frac{E_{lossPath3}}{\eta_{\text{BT-CH/DCH}}} \tag{14}$$

F. Sizing of the Battery

The first step in sizing the battery is identifying its voltage level, especially in the case of unregulated bus voltage. This might be adjusted by identifying the battery technology and number of cells that can be installed in the string $N_S = v_{BusNom}/v_{cellNom}$. Regarding the battery capacity, it is identified based on the battery energy and can be adjusted by considering the string voltage $C_{BT}(\text{Ah}) = E_{BT}(\text{Wh})/v_{BusNom}$ and number of strings $N_P = C_{BT}/(C_{cell} N_S)$. Another important parameter in the battery selection, especially from its reliability point of view, is the maximum allowed level of the DOD, which relates the battery energy to the energy to be supplying the payloads during the eclipse time interval $\text{DOD} = E_{load}^{eclipse}/E_{BT}$. Since the high discharging current may affect the life time of the battery, where this latter has to be designed considering the cases of high-power pulsed loads, where a possible solution could be by adding more strings.

G. Sizing of the solar array

The solar energy must always meet the balance expressed by (1) with an additional margin, even at the end-of-life (EOL). This energy is calculated by integrating the PV harvested power during the sunlight, which its self is dependent on the solar array equivalent area (A_{PV}^{eq}) and average solar irradiance in the space (G_{AM0}, W/m^2), as well as the solar cells efficiency ($\eta_{Sun/PV}$), where the former denotes to the solar cells area that is perpendicular to the sun radiation during the whole orbit. In these parameters, the PV solar array efficiency and solar irradiance can be considered to be constrained, while the solar array equivalent area is flexible, and can be estimated as

$$A_{\text{PV}}^{eq} = \frac{E_{\text{PV}}}{\int_{t_{\text{ini}}}^{t_{\text{ini}}+t_{\text{eclipse}}} P_{\text{PV}}(\text{t})\, dt} = \frac{E_{\text{PV}}}{G_{\text{AM0}}\ \eta_{Sun/\text{PV}}} \tag{15}$$

The PV solar array as function of the equivalent one can be expressed as

$$A_{\text{PV}}^{eq} = \int_{t_{\text{ini}}}^{t_{\text{ini}}+t_{\text{eclipse}}} A_{\text{PV}}(\text{t})\, dt \tag{16}$$

In the case of a CubeSat, where the solar cells are installed on all the facets, an approximation of the solar array equivalent area could be made by using the projected areas of the cube. In space, the CubeSat may be oriented with respect to the sun in three different positionings, based on which the facets subjected to the sun vary in count and angles. In the case of only one facet is subjected to the sun, then the solar array area would be A_{Facet}, which is increased to $\sqrt{2}\ A_{Facet}$ if two adjacent facets are facing the sunlight,

while for the case of the vertex is facing the sunlight it would be increased to $\sqrt{3}A_{\text{Facet}}$. By averaging those PV solar arrays areas, the equivalent one is deduced as $A_{\text{PV}}^{eq} = 1.38A_{\text{Facet}}$.

VII. Conclusion

This paper provided an overview on the technical architectures and different parts of the EPS for CubeSats. Among which the energy generation and storage, as well as the protection system. It has been shown that triple junction solar cells GaInP/GaAs/Ge are the ones being employed in the space industry due to their higher efficiency. In addition, GaInP/GaAs/Ge triple junction solar cells generate power under higher voltage compared to Si-based ones. Regarding the storage systems, it was revealed that Li-Ion battery technology has replaced the NiCd. This is due to the higher efficiency, reliability, and power density that they offer. Besides, Li-ion batteries suffer from a lower burden from the memory perspective. Finally, sizing guidelines of the energy generation and storage systems were also provided considering the orbit duration, load demand, and power loss in the overall EPS.

VIII. For Further Reading

J. Bouwmeester and J. Guo, "Survey of worldwide pico-and nanosatellite missions, distributions and subsystem technology," *Acta Astronaut.*, vol. 67, no. 7-8, pp. 854-862 2010.

A. Aoudeche, X. Zhao and K.D. Kerrouche, "Design of a High Performance Electrical Power System for an Earth Observation Nano-Satellite," in Proceedings of the 2018 International Conference on Electronics and Electrical Engineering Technology, 2018, pp. 140-146.

P. Bugryniec, "Cubesat: The need for more power to realise telecommunications," *final report of mini project, University of Sheffield* 2016.

T. Komarek, Z. Bailey, H. Schone, T. Jedrey, A. Chandler, "Novel ideas for exploring Mars with CubeSats: challenges and possibilities ," *Proc. of the 10th Low-cost planetary missions conference*, Pasadena, California, 18-20 Jun. 2013.

E. Kulu, Nanosats Database. [Online]. Available: https://www.nanosats.eu/. [Accessed: 20-Jul-2020].

Lee, Jinkyu, Eugene Kim, and Kang G. Shin. "Design and management of satellite power systems." *In 2013 IEEE 34th Real-Time Systems Symposium*, pp. 97-106. IEEE, 2013.

Lim, Timothy M., Aaron M. Cramer, James E. Lumpp, and Samir A. Rawashdeh. "A modular electrical power system architecture for small spacecraft." *IEEE Transactions on Aerospace and Electronic Systems* 54, no. 4 (2018): 1832-1849.

Djebko, Kirill, Frank Puppe, and Hakan Kayal. "Model-based fault detection and diagnosis for spacecraft with an application for the SONATE triple cube nano-satellite." *Aerospace* 6, no. 10 (2019): 105.

Pang, Chee Khiang, Akash Kumar, Cher Hiang Goh, and Cao Vinh Le. "Nano-satellite swarm for SAR applications: Design and robust scheduling." *IEEE Transactions on Aerospace and Electronic Systems* 51, no. 2 (2015): 853-865.

Bester, Jean, Ben BJ Groenewald, and Richardt H. Wilkinson. "Electrical power system for a 3U CubeSat nanosatellite incorporating peak power tracking with dual redundant control." (2012).

Ali, Anwar, M. Rizwan Mughal, Haider Ali, and Leonardo Reyneri. "Innovative power management, attitude determination and control tile for CubeSat standard NanoSatellites." Acta Astronautica 96 (2014): 116-127.

A. Lashab, D. Sera and J. M. Guerrero, "A Dual-Discrete Model Predictive Control-Based MPPT for PV Systems," *IEEE Trans. Power Electron.*, vol. 34, no. 10, pp. 9686-9697, Oct. 2019, doi: 10.1109/TPEL.2019.2892809.

A. Lashab, D. Sera, J. Martins and J. M. Guerrero, "Dual-Input Quasi-Z-Source PV Inverter: Dynamic Modeling, Design, and Control," in *IEEE Transactions on Industrial Electronics*, vol. 67, no. 8, pp. 6483-6493, Aug. 2020.

M. Schmidt, K. Ravandoor, O. Kurz, S. Busch, K. Schilling, "Attitude determination for the pico-satelliteUWE-2," *Proceedings of the 17th World Congress, The International Federation of Automatic Control*, Seoul, Korea, 6–11 July 2008.

S. P. Viswanathan and A. Sanyal, "Design of an Adaptive Singularity-free Control Moment Gyroscope (ASCMG) actuator for agile and precise attitude control of cubesat," *2016 Indian Control Conference* (ICC), Hyderabad, 2016, pp. 284-291.

C. Kaplan, "LEO Satellites: Attitude Determination and Control Components, Some Linear Attitude Control Techniques," A Thesis Submitted to the Graduate School of Natural and Applied Sciences of Middle East Technical University.

E. Wertheimer, L. Berthoud, M. Johnson, "PocketRTG – a cubesat scale radioisotope thermoelectric generator using COTS fuel," *iCubeSat Workshop,* 2015.

M. G. Villalva, J. R. Gazoli and E. R. Filho, "Comprehensive Approach to Modeling and Simulation of Photovoltaic Arrays," *IEEE Transactions on Power Electronics*, vol. 24, no. 5, pp. 1198-1208, May 2009.

A. Lashab, A. Bouzid and H. Snani, "Comparative study of three MPPT algorithms for a photovoltaic system control," 2015 *World Congress on Information Technology and Computer Applications* (WCITCA), Hammamet, 2015, pp. 1-5, doi: 10.1109/WCITCA.2015.7367039.

M. Robyn, L. Thaller, and D. Scott, "Nanosatellite power system considerations," *Proceedings of the International Conference on Integrated Micro/Nanotechnology for Space Applications*, Oct 30–Nov 3, 1995, 259–265.

S.-J. Kang and H.-U. Oh, "On-Orbit Thermal Design and Validation of 1 U Standardized CubeSat of STEP Cube Lab," *International Journal of Aerospace Engineering*, vol. 2016, pp. 1–17, 2016.

G. F. Volpi, "Power Line Protection Devices in Space Applications," *EUROCON 2007 - The International Conference on "Computer as a Tool"*, Warsaw, 2007, pp. 1636-1640.

N. Navarathinam, R. Lee, H. Chesser, Characterization of Lithium-Polymer batteries for CubeSat applications, *Acta Astronautica*, Vol. 68, PP 1752-1760, 2011.